Richard L. Larock for comments, and Dr. Giorgio Cerichelli for the ^{13}C NMR experiments. We are also grateful to Aurelia Stella for typing the manuscript.

Registry No. 1, 501-65-5; (*E*)-**2a**, 127971-26-0; (*Z*)-**2a**, 127971-27-1; (*E*)-**3a**, 127971-30-6; (*Z*)-**3a**, 127971-31-7; (*E*)-**3b**, 19191-03-8; (*Z*)-**3b**, 19202-54-1; **3c**, 451-40-1; **4a**, 127971-28-2; **5a**, 127971-29-3; mercury(II) acetate, 1600-27-7; mercury(II) trifluoroacetate, 13257-51-7.

Supplementary Material Available: Listings of thermal parameters for **4a** and **5a** (1 page); listings of observed and calculated structure factors (25 pages). Ordering information is given on any current masthead page.

EPR Studies of $M(CO)_5^-$ Radicals (M = Cr, Mo, W) Trapped in Single Crystals of $PPN^+HM(CO)_5^-$ †

Rosemary C. Hynes, Keith F. Preston,* Jerry J. Springs, and Antony J. Williams

Division of Chemistry, National Research Council of Canada, Ottawa, Ontario, Canada K1A 0R6

Received January 16, 1990

γ-Irradiated single crystals of $PPN^+HM(CO)_5^-$ (M = Cr, Mo, W) exhibit persistent anisotropic EPR spectra that are assigned to the free radical ($S = {}^1/_2$) anion metal carbonyls $M(CO)_5^-$. Measurements of the *g* and metal hyperfine interaction anisotropies in crystallographically aligned single-crystal specimens at 77 K are consistent with square-pyramidal geometries for the radicals and unpaired spin densities largely confined to metal d_{z^2} atomic orbitals. A full structure of the W-containing host crystal was established by X-ray diffractometry (space group $P2_1/c$, a = 13.302 (11) Å, b = 20.041 (15) Å, c = 16.074 (7) Å, β = 102.56 (6)°, Z = 4), and unit cell parameters were measured for the isomorphous Cr (a = 13.2413 (22) Å, b = 20.1480 (24) Å, c = 15.9510 (20) Å, β = 102.33 (12)°) and Mo (a = 13.266 (18) Å, b = 20.09 (5) Å, c = 16.07 (8) Å, β = 102.57 (8)°) hosts. In spite of a poor structural refinement (R = 0.13), attributed to high thermal motion and crystal decay, the correlation of tensor principal directions with crystallographic directions was very good. In the case of the Cr compound, a further weak EPR spectrum is ascribed to an antiferromagnetically coupled pair of $Cr(CO)_5^-$ radicals that corresponds to one specific pair of nearest neighbor anions in the crystal structure.

Introduction

The structures of pentacoordinate transition-metal complexes hold a particular fascination for spectroscopists because of the near equality in energy of square-pyramidal and trigonal-bipyramidal geometries and the ease of interconversion between them.[1] In many instances, the pentacoordinate species are reactive intermediates on the pathway between tetracoordinate and hexacoordinate complexes, and their spectroscopic detection calls for special isolation techniques. Our particular interest lies in paramagnetic transition-metal carbonyls, which we endeavor to trap in single-crystal hosts for subsequent examination by electron paramagnetic resonance (EPR) spectroscopy.[2] One of the first investigations that we undertook in this area was the study[3] of the $Fe(CO)_5^+$ radical cation produced by γ-irradiation of the neutral carbonyl trapped in single crystals of $Cr(CO)_6$. Examination of the **g**, ^{13}C hyperfine, and ^{57}Fe hyperfine tensors proved conclusively that the radical in $Cr(CO)_6$ had square-pyramidal geometry with much of the unpaired spin density located in a Fe $3d_{z^2}$ orbital. This conclusion reinforced inferences drawn from contemporary powder spectroscopic studies that the isoelectronic species $Mn(CO)_5$,[4-10] $Re(CO)_5$[11-13] and $M(CO)_5^-$ (M = Cr, Mo, W)[14] also have C_{4v} geometry. Phosphine-substituted manganese[15] and rhenium[16] carbonyls appear to retain this geometry, whereas phosphine-substituted iron carbonyl cations and acyl-substituted iron carbonyls[17] adopt a trigonal-bipyramidal geometry.

In order to explore the geometry and electronic structure of the group 6 pentacarbonyl anion radicals, we chose to examine[18] radiation-damaged single crystals of PPh_4^+-$HCr(CO)_5^-$. To our surprise, the radical $Cr(CO)_5^-$ in that

Table I. Summary of X-ray Diffraction Data

compd	$PPN^+HW(CO)_5^-$
formula	$C_{41}H_{31}NO_5P_2W$
fw	863.50
a, Å	13.302 (11)
b, Å	20.041 (15)
c, Å	16.074 (7)
α, deg	90.00
β, deg	102.56 (6)
γ, deg	90.00
V, Å^3	4182.5
Z	4
ρ_{calcd}, g cm^{-3}	1.371
space group	$P2_1/c$
cryst dimens, mm	0.40 × 0.40 × 0.07
temp, °C	18
radiation	Mo Kα
μ, cm^{-1}	29.4
data collection	ω-2θ
max 2θ, deg	42.0
scan speed, deg min^{-1}	2
scan width, deg	1
total no. of observns	5340
no. of unique data, $I > 2.5\sigma(I)$	2031
final no. of variables	261
final max shift/error	1.198
max residual density, e Å^{-3}	1.79
R^a	0.132
R_w^b	0.157

$^a \sum||F_o| - |F_c||/\sum|F_o|$. $^b [\sum w(|F_o| - |F_c|)^2/\sum wF_o^2]^{1/2}$.

† NRCC No. 31844.

(1) Rossi, A. R.; Hoffmann, R. *Inorg. Chem.* **1975**, *14*, 365.
(2) Symons, M. C. R.; Morton, J. R.; Preston, K. F. *ACS Symp. Ser.* **1987**, *No. 333*, 169.

0276-7333/90/2309-2298$02.50/0 Published 1990 by the American Chemical Society

Table II. Atomic Parameters x, y, z and Temperature factors B_{iso} for $PPN^+HW(CO)_5^-$[a,b]

	x	y	z	B_{iso}, Å^2
W	0.81002 (15)	0.87852 (9)	0.01808 (11)	4.45 (8)
P(1)	0.2237 (8)	0.6881 (5)	0.0433 (6)	3.4 (5)
P(2)	0.4324 (8)	0.6993 (5)	0.0119 (6)	3.2 (4)
O(1)	0.695 (3)	0.9038 (21)	0.1627 (20)	8.9 (25)
O(2)	0.919 (3)	0.7605 (24)	0.1126 (23)	10.4 (26)
O(3)	0.9338 (23)	0.8585 (24)	−0.1285 (20)	8.6 (24)
O(4)	0.663 (3)	0.9564 (16)	−0.0917 (23)	9.6 (22)
O(5)	0.969 (3)	0.9919 (17)	0.0957 (21)	7.2 (18)
N	0.3357 (21)	0.6693 (14)	0.0211 (17)	2.9 (6)
C(1)	0.727 (3)	0.8922 (18)	0.1080 (22)	3.0 (7)
C(2)	0.889 (4)	0.8291 (24)	0.049 (3)	6.9 (10)
C(3)	0.887 (3)	0.8718 (23)	−0.082 (3)	5.2 (10)
C(4)	0.722 (4)	0.9210 (24)	−0.016 (3)	6.2 (10)
C(5)	0.915 (3)	0.9509 (20)	0.059 (3)	4.2 (8)

[a] Partial listing only; full listing in supplementary material. [b] Estimated standard deviations in parentheses refer to last significant digit.

host occurred almost exclusively as radical pairs of nearest-neighbor damaged anions. While the spin–spin interactions within the isolated radical pairs are of great interest in themselves, we naturally sought alternative hosts for the monoradical that were uncomplicated by the presence of biradical pairs. In this paper we discuss the structure of the radical anions $M(CO)_5^-$ (M = Cr, Mo, W) as deduced from anisotropic EPR spectra observed in single crystals of $PPN^+HM(CO)_5^-$ ($PPN^+ \equiv (Ph_3P)_2N^+$).

Experimental Section

(a) Preparation. All preparations were performed according to published literature procedures.[19] Solvents were purified by distillation from sodium–benzophenone ketyl or bought as reagent grade. Single crystals of $PPN^+HM(CO)_5^-$ (M = Cr, Mo, W) grown from hexane and tetrahydrofuran were either orange needles (Cr and Mo) or yellow needles (W).

(b) Crystallography. X-ray diffraction data (Table I) were collected for a crystal of the tungsten compound on an Enraf-Nonius CAD diffractometer controlled by NRCCAD software. The intensities of three standard reflections dropped by half during the course of data collection, indicating significant crystal decay. Furthermore, high thermal motion prevented observations for $2\theta > 42°$, so that a limited data set was obtained. The linear absorption coefficient and the crystal size were such (Table I) that an absorption correction was not considered essential in view of the crystal degradation that occurred over the data collection time. The structure was solved by direct methods, which gave the positions of the tungsten and two phosphorus atoms; a difference Fourier calculation revealed all other non-hydrogen atoms. A second difference Fourier calculation showed a collection of five peaks that were rationalized as a partial solvent tetrahydrofuran (THF) molecule. These were included in the atom list with the largest peak assigned to oxygen; they were fixed thermally and their positional parameters and occupancies refined. All five atoms were refined to occupancies of ca. 0.6. Hydrogen atom positions were included in the idealized geometries and in the calculation of structure factors, but they were not refined. No attempt was made to locate the hydride ion. Data reduction, structure solution, and refinement were all carried out with use of the NRCVAX system of crystal-structure programs.[20] A partial listing of positional and thermal parameters for atoms appears in Table II, and selected bond angles, distances, and directions are given in Table III. A rigid-body refinement was also carried out for ideal rings, straight W–C–O linkages, and the expected bond lengths. The results of this refinement are deposited as supplementary material along with complete listings of structural data.

The unit cell parameters for each of the compounds were determined at the time of alignment prior to EPR spectroscopy, but a full crystal structure was extracted for the tungsten com-

Table III. Selected[a] Bond Distances (Å) and Angles (deg) for $PPN^+HW(CO)_5^-$

a. Distances

W–C(1)	2.01 (3)	W–C(2)	1.45 (5)
W–C(3)	2.09 (4)	W–C(4)	1.45 (5)
W–C(5)	2.03 (4)	P(1)–N	1.65 (3)
P(2)–N	1.46 (3)	O(1)–C(1)	1.09 (5)
O(2)–C(2)	1.71 (7)	O(3)–C(3)	1.10 (5)
O(4)–C(4)	1.48 (7)	O(5)–C(5)	1.16 (5)

b. Angles

C(1)–W–C(2)	108.6 (21)	C(1)–W–C(3)	174.3 (16)
C(1)–W–C(4)	70.7 (21)	C(1)–W–C(5)	96.6 (15)
C(2)–W–C(3)	77.1 (22)	C(2)–W–C(4)	172 (3)
C(2)–W–C(5)	89.0 (22)	C(3)–W–C(4)	103.7 (22)
C(3)–W–C(5)	83.0 (17)	C(4)–W–C(5)	98.4 (22)
P(1)–N–P(2)	141.9 (20)	W–C(1)–O(1)	170 (4)
W–C(2)–O(2)	144 (3)	W–C(3)–O(3)	168 (4)
W–C(4)–O(4)	146 (4)	W–C(5)–O(5)	168 (3)

c. Least-Squares Planes

plane 1: $[6.91\ (19)]x + [15.4\ (3)]y + [4.1\ (3)]z = 19.19\ (16)$

distances (Å) to plane from the atoms in the plane

W	0.000 (3)	C(1)	0.01 (4)	C(2)	−0.09 (6)
C(3)	0.01 (5)	C(4)	−0.09 (6)		

plane 2: $[6.96\ (19)]x + [15.5\ (3)]y + [4.1\ (3)]z = 19.17\ (17)$

distances (Å) to plane from the atoms in the plane

C(1)	0.03 (5)	C(3)	0.05 (6)	C(4)	−0.06 (6)
C(2)	−0.06 (6)				

[a] Full listing provided in supplementary material.

Table IV. Comparison of Unit Cell Parameters for $PPN^+HM(CO)_5^-$ (M = Cr, Mo, W)

compd	a, Å	b, Å	c, Å	β, deg
$PPN^+HCr(CO)_5^-$	13.2413 (22)	20.1480 (24)	15.9510 (20)	102.33 (12)
$PPN^+HMo(CO)_5^-$	13.266 (18)	20.09 (5)	16.07 (8)	102.57 (8)
$PPN^+HW(CO)_5^-$	13.302 (11)	20.041 (15)	16.074 (7)	102.56 (6)

(3) Lionel, T.; Morton, J. R.; Preston, K. F. *J. Chem. Phys.* **1982**, *76*, 234.
(4) Huber, H.; Kündig, E. P.; Ozin, G. A.; Poë, A. J. *J. Am. Chem. Soc.* **1975**, *97*, 308.
(5) Howard, J. A.; Morton, J. R.; Preston, K. F. *Chem. Phys. Lett.* **1981**, *83*, 226.
(6) Church, S. P.; Poliakoff, M.; Timney, J. A.; Turner, J. J. *J. Am. Chem. Soc.* **1981**, *103*, 7515.
(7) Symons, M. C. R.; Sweany, R. L. *Organometallics* **1982**, *1*, 834.
(8) Yesaka, H.; Kobayashi, T.; Yasufuku, K.; Nagakura, S. *J. Am. Chem. Soc.* **1983**, *105*, 6249.
(9) Church, S. P.; Hermann, H.; Grevels, F.-W.; Schaffner, K. *J. Chem. Soc., Chem. Commun.* **1984**, 785.
(10) Kobayashi, T.; Yasufuku, K.; Iwai, J.; Yesaka, H.; Noda, H.; Ohtani, H. *Coord. Chem. Rev.* **1985**, *64*, 1.
(11) Meckstroth, W. K.; Walters, R. T.; Waltz, W. L.; Wojcicki, A.; Dorfman, L. M. *J. Am. Chem. Soc.* **1982**, *104*, 1842.
(12) Yasufuku, K.; Noda, H.; Iwai, J.; Ohtani, H.; Hoshino, M.; Kobayashi, T. *Organometallics* **1985**, *4*, 2174.
(13) Kobayashi, T.; Ohtani, H.; Noda, H.; Teratani, S.; Yamazaki, H.; Yasufuku, K. *Organometallics* **1986**, *5*, 110.
(14) Breeze, P. A.; Burdett, J. K.; Turner, J. J. *Inorg. Chem.* **1981**, *20*, 3369.
(15) Kidd, D. R.; Cheng, C. P.; Brown, T. L. *J. Am. Chem. Soc.* **1978**, *100*, 4103. McCullen, S. B.; Brown, T. L. *J. Am. Chem. Soc.* **1982**, *104*, 7496.
(16) Walker, H. W.; Rattinger, G. B.; Belford, R. L.; Brown, T. L. *Organometallics* **1983**, *2*, 775.
(17) Krusic, P. J.; Cote, W. J.; Grand, A. *J. Am. Chem. Soc.* **1984**, *106*, 4642. Therien, M. J.; Trogler, W. C. *J. Am. Chem. Soc.* **1986**, *108*, 3697.
(18) Morton, J. R.; Preston, K. F.; Darensbourg, M. Y. *Magn. Reson. Chem.* **1988**, *26*, 787.
(19) Darensbourg, M. Y.; Deaton, J. C. *Inorg. Chem.* **1981**, *20*, 1644. Darensbourg, M. Y.; Slater, S. *Inorg. Synth.* **1983**, *22*, 181. Darensbourg, M. Y.; Bau, R.; Marks, M. W.; Burch, R. R., Jr.; Deaton, J. C.; Slater, S. *J. Am. Chem. Soc.* **1982**, *104*, 6961.
(20) Gabe, E. J.; Le Page, Y.; Charland, J.-P.; Lee, F. L.; White, P. S. *J. Appl. Crystallogr.* **1989**, *22*, 384.

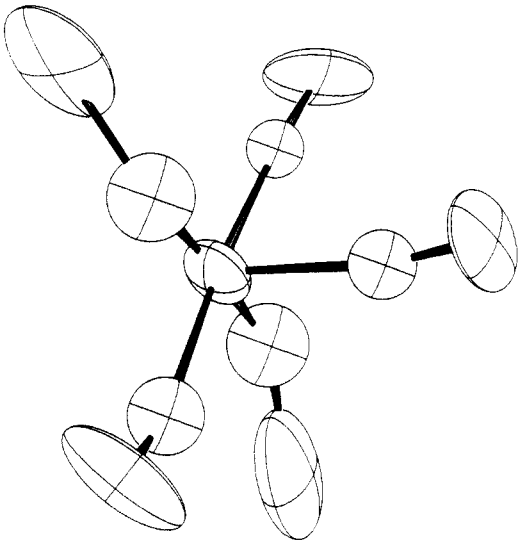

Figure 1. ORTEP view of the anion in $PPN^+HW(CO)_5^-$.

pound only. Since the three compounds are isomorphous (see Table IV), this single-crystal structure was deemed sufficient to allow comparison of certain directions within each crystal with the extracted **g**-tensor principal directions.

Single crystals were irradiated at 77 K in a 400-TBq ^{60}Co source. The radical generated was stable at room temperature for several days, enabling the crystals to be aligned absolutely on a Picker diffractometer according to the structural parameters. These crystals were glued inside the ends of 4-mm quartz tubes with one of the orthogonal axes a^*bc of the $P2_1/c$ monoclinic crystal aligned parallel to the length of the tube and the direction of one of its other axes being indicated by a pointer attached to the tube. Contact of the crystals with air was minimized by coating them with epoxy glue in a drybox prior to alignment.

(c) EPR Spectroscopy. EPR spectra were obtained with a Varian Associates E-12 spectrometer. Magnetic field intensity was determined with a Bruker ER-035M gauss meter and microwave frequency with a Systron-Donner digital counter. With the quartz tube and affixed crystal placed in the cold-finger Dewar inside the microwave cavity of the spectrometer, the pointer lay over a horizontal brass protractor graduated every 5° of arc. By rotation of the tube about its long axis the magnetic field of the spectrometer could then explore a crystallographic plane. Three separate planes, a^*b, a^*c, and bc, were explored together with a skew direction in order to characterize the monoclinic unit cell.[21]

Results

(a) Crystal Structure. In the $HW(CO)_5^-$ anion, the geometry of the carbonyl ligands about tungsten is approximately square pyramidal (Figures 1 and 2). The hydride ion is assumed to occupy the sixth site at tungsten, completing the octahedral environment about the metal nucleus. A least-squares plane calculated for the tungsten and the coordinated carbons showed no significant deviation from planarity. However, two of the W–C distances are unreasonably short (1.45 Å), the corresponding C–O bonds are unreasonably long (1.7, 1.5 Å), and the W–C–O angles are ca. 145°. These distortions from the expected[19] geometry are undoubtedly artifacts of the poor refinement and high thermal motion within the ion, which is also reflected in the large thermal parameters for the oxygens and, to a lesser extent, for the carbonyl carbons. Fortunately, these distortions did not influence the correlation established between bond and tensor directions (see below): use of the results of a rigid-body refinement (supplementary material) did not alter the conclusions based upon the full refinement. Variations in the carbon–carbon

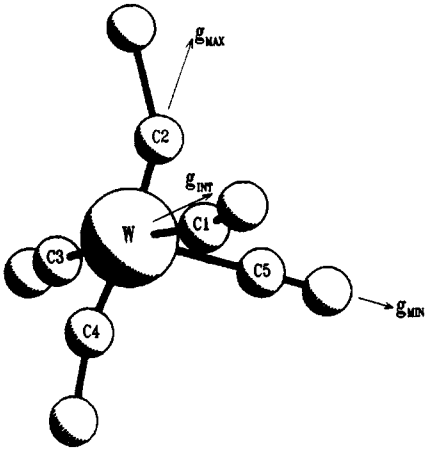

Figure 2. Structure of the $HW(CO)_5^-$ anion in $PPN^+HW(CO)_5^-$, showing the directions of the principal g values of the radical $W(CO)_5^-$. Hydrogen atom positions were not determined. Structures for the Cr and Mo congeners are almost identical.

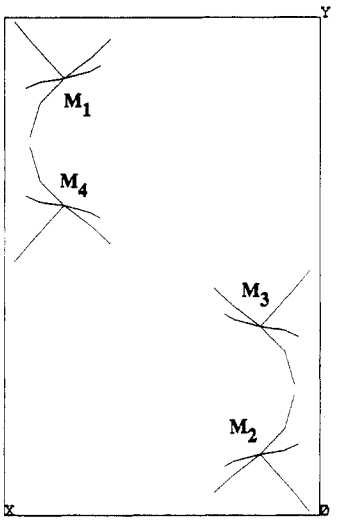

Figure 3. Unit cell of $PPN^+HW(CO)_5^-$ projected along $Z(c)$, showing anions (except the hydrogen atoms) only. Labels M_{1-4} refer to the four sites.

bond lengths within the phenyl rings of the cation were another symptom of poor data. Otherwise, the geometry of the PPN^+ cation was unremarkable.

(b) ESR Spectra. For an arbitrary orientation of the dc magnetic field, each of the radiation-damaged crystals $PPN^+HM(CO)_5^-$ (M = Cr, Mo, W) showed an EPR spectrum consisting of two equally intense lines. Their resonant magnetic fields were markedly anisotropic, and for certain orientations they coalesced to a single line. Such behavior is typical[21] of an electronic doublet substitutional impurity in a monoclinic host: the two components of the EPR spectrum correspond to two magnetically inequivalent sites for a radical impurity that has a skew orientation in the monoclinic unit cell (Figure 3). Since the compounds all crystallized in the monoclinic system (Table IV), this observation shows that the impurity centers obeyed the host crystal symmetry (space group $P2_1/c$).

g^2 values were measured for each site and were plotted (see for example Figure 4) against the angle for each crystal plane. Matrix elements of the $\mathbf{g}^2$ tensor were obtained from[21] least-squares fits of expressions of the type

$$g^2(\theta) = g_{xx}^2 \sin^2\theta + g_{yy}^2 \cos^2\theta + g_{xy}^2 \sin 2\theta$$

to the experimental data. Relative signs of the off-diagonal elements for the a^*b and bc planes were established[21] from

(21) Morton, J. R.; Preston, K. F. *J. Magn. Reson.* **1983**, *52*, 457.

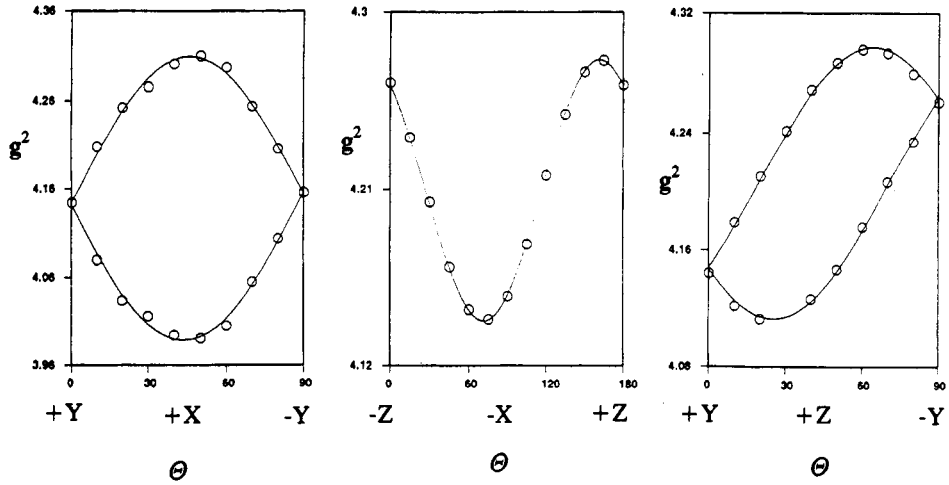

Figure 4. Plots of g^2 values for $W(CO)_5^-$ as a function of angle in the three crystal planes of $PPN^+HW(CO)_5^-$ and best-fit sinusoidal curves to the data.

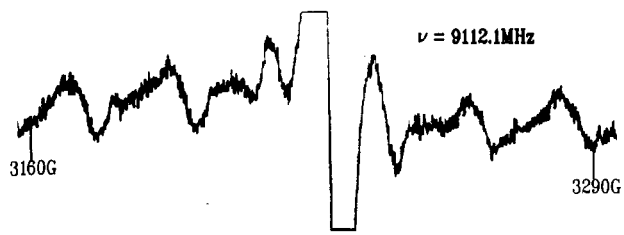

Figure 5. First-derivative EPR spectrum of the $Mo(CO)_5^-$ radical for $B_0 \| X(a^*)$ in the $PPN^+HMo(CO)_5^-$ crystal at 77 K, showing the $^{95,97}Mo$ hyperfine manifold.

Table V. g^2 and $g \cdot D \cdot g$/MHz Tensors for the $Cr(CO)_5^-$ Radical and Radical Ion Pair in a $PPN^+HCr(CO)_5^-$ Crystal: Principal Values of g and D (MHz) and Their Direction Cosines in the a^*bc Axis System

	tensor			direction cosines		
				x =	y =	z =
	a^*	b	c	2.0215	2.0203	2.0020
g^2	4.0543	±0.0345	−0.0169	0.7500	0.1744	0.6380
	±0.0345	4.0467	±0.0156	±0.4682	±0.5413	∓0.6984
	−0.0169	±0.0156	4.0749	−0.4672	0.8225	0.3243

	tensor			direction cosines		
	a^*	b	c	x = 38.4	y = 34.6	z = −73.9
$g \cdot D \cdot g$	142.4	0	9.1	0.3968	0.9169	−0.0183
	0	56.1	∓185.6	∓0.8106	±0.3617	±0.4606
	9.1	∓185.6	−205.1	0.4289	−0.1689	0.8874

$|D|$ = 110.9 MHz; $|E|$ = 1.9 MHz

a comparison of predicted and measured g^2 values for a skew (1, 1, 1) direction in the a^*bc basis. The experimental tensors, principal values, and directions are given in Tables V–VII.

Weak satellite resonances were detected in the spectra observed in the Cr and Mo compounds. In the Mo case, six equally spaced satellites were (Figure 5) centered about each strong resonance with relative intensities appropriate for the natural content of magnetic Mo isotopes (15.9% ^{95}Mo, $I = {}^5/_2$; 9.6% ^{97}Mo, $I = {}^5/_2$). Accordingly, they were attributed to Mo hyperfine interaction with a single magnetic Mo nucleus. Line width limitations coupled with the small difference in magnetogyric ratios (≃2%) unfortunately prevented resolution of the individual ^{95}Mo and ^{97}Mo hyperfine manifolds. From measurements of the hyperfine splitting as a function of angle in each crystal plane, plots of g^2a^2 were drawn up and the elements of the $\mathbf{g \cdot a^2 \cdot g}$ tensor were assembled in the manner described above for $\mathbf{g}^2$. The Mo hyperfine interaction tensor, prin-

Table VI. g^2 and $g \cdot a^2 \cdot g$/MHz² Tensors for the $Mo(CO)_5^-$ Radical in a $PPN^+HMo(CO)_5^-$ Crystal: Principal Values of g and Hyperfine Interaction[a] (MHz) and Their Direction Cosines in the a^*bc Axis System

	tensor			direction cosines		
				x =	y =	z =
	a^*	b	c	2.0264	2.0241	2.0009
g^2	4.0603	±0.0476	−0.0138	0.6299	0.4156	0.6562
	±0.0476	4.0543	±0.0191	±0.7021	±0.0566	∓0.7098
	−0.0138	±0.0191	4.0919	0.3321	0.9078	0.2561

	tensor			direction cosines		
	a^*	b	c	x = 0	y = 28.7	z = 103.1
$g \cdot a^2 \cdot g^a$	17944	∓20240	5794	0.7597	0.0017	0.6503
	∓20240	22927	∓5600	±0.6256	∓0.2748	∓0.7302
	5794	∓5600	4990	−0.1775	−0.9615	0.2099

[a] Hyperfine measurements and parameters refer to an average for the ^{95}Mo and ^{97}Mo isotopes, since their satellite spectra were not resolved from each other.

Table VII. g^2 Tensor for the $W(CO)_5^-$ Radical in a $PPN^+HW(CO)_5^-$ Crystal: Principal Values of g and Their Direction Cosines in the a^*bc Axis System

	tensor			direction cosines		
				x =	y =	z =
	a^*	b	c	2.0791	2.0671	1.9925
g^2	4.1562	±0.1595	−0.0389	0.5452	0.5179	0.6592
	±0.1595	4.1457	±0.0720	±0.6867	±0.1752	∓0.7055
	−0.0389	±0.0720	4.2641	0.4809	−0.8373	0.2601

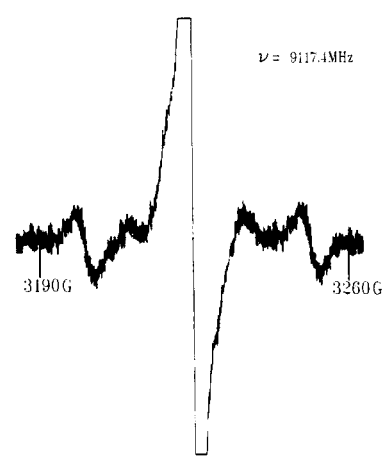

Figure 6. First-derivative EPR spectrum of the $Cr(CO)_5^-$ radical for $B_0 \| Z(c)$ in the $PPN^+HCr(CO)_5^-$ crystal at 77 K, showing the weak absorptions due to the triplet radical pair.

Table VIII. Comparison of the Single-Crystal g Values with Those for Liquid and Frozen 2-MeTHF

radical	cryst				2-MeTHF glass[b]		soln[b]
	g_{xx}	g_{yy}	g_{zz}	g_{av}[a]	$g_\perp$	$g_\parallel$	g_{iso}
$Cr(CO)_5^-$	2.0215	2.0203	2.0020[c]	2.0146	2.0205	2.0019	2.0143
	2.0199	2.0199	2.0021[d]				
$Mo(CO)_5^-$	2.0264	2.0241	2.0009[c]	2.0171	2.0246	2.0010	2.0167
	2.0230	2.0230	2.0006[d]				
$W(CO)_5^-$	2.0791	2.0671	1.9925[c]	2.0462	2.0709	1.9921	2.0449
	2.0676	2.0676	1.9906[d]				

[a] Calculated from $(g_{xx} + g_{yy} + g_{zz})/3$. [b] Reference 22. [c] Values for $PPN^+HM(CO)_5^-$. [d] Values for $PPh_4^+HM(CO)_5^-$ from refs. 18 and 28.

cipal values, and directions are given in Table VI.

In the Cr-containing crystal, a pair of satellites (Figure 6) centered about each principal resonance were detected. Tentatively, these were treated as the outside ($m_I = \pm 1.5$) lines of a ^{53}Cr ($I = {}^3/_2$) hyperfine manifold, assuming that the inner pair were "lost" in the central resonance. However, the resulting values of g^2a^2 did not fit a sinusoidal relationship unless certain of them were changed in sign. Since negative values of g^2a^2 are clearly impossible, it was concluded that the pair of satellites arose from a spin–spin interaction rather than a nuclear hyperfine interaction. Accordingly, plots of $\beta g^3(\Delta B)/3$ against angle were generated from the observed separation of the satellites in magnetic field intensity, ΔB. Such plots were sinusoidal within error and led to the matrix elements of the tensor $\mathbf{g}\cdot\mathbf{D}\cdot\mathbf{g}$, where $\mathbf{D}$ is the fine-structure tensor (Table V).[18]

No satellite lines could be found for the tungsten signals, in spite of the 14% natural content of magnetic tungsten (^{183}W, $I = {}^1/_2$). This was attributed to the weakness of the spectrum in $PPN^+HW(CO)_5^-$ and the large line width of the signal (p–p width 9.4 G for B_0 parallel to a^*, compared to 6.0 G in Cr and 5.4 G in Mo).

Discussion

The principal g values of the three radicals observed in the radiation-damaged crystals and their averages are compared in Table VIII with the values determined in the single-crystal hosts[18,28] $PPh_4^+HM(CO)_5^-$ (M = Cr, Mo, W) and from spectra generated[22] in frozen 2-MeTHF and in liquid THF by the ultraviolet photolysis of $K_2M_2(CO)_{10}$ (M = Cr, Mo, W). The close similarity of the values for the single-crystal hosts and for 2-MeTHF solutions leaves little doubt that they refer to the same species. From considerations of the $\mathbf{g}$ tensors and the metal and ^{13}C hyperfine interactions, Krusic[22] assigned the spectra observed in solution to square-pyramidal 17-electron metal carbonyl anions, $M(CO)_5^-$, which arose through photolytic cleavage of the metal–metal bond in the binuclear reagents. Such radicals are also anticipated products of radiation damage of the $HM(CO)_5^-$ anions, so that our present observations support this contention. Furthermore, our determinations of principal directions of $\mathbf{g}$ and metal hyperfine interaction tensors confirm the assignment to an a_1 SOMO in C_{4v} geometry with substantial unpaired spin density in the metal d_{z^2} orbital.

In associating the experimentally determined principal $\mathbf{g}$-tensor directions with crystallographic directions, it is important to realize that the tensors for $Cr(CO)_5^-$ and $Mo(CO)_5^-$ are very nearly axial (Table VIII). It is doubtful if much significance can be attached to the principal directions for g_{xx} and g_{yy} in those cases, therefore. A rhombic $\mathbf{g}$ tensor is permitted in the low site symmetry of the monoclinic crystals, of course, and is quite clearly established for the case of $W(CO)_5^-$. In glassy 2-MeTHF[22] and in higher symmetry hosts,[18,28] all of the radicals adopt the axial symmetry anticipated for the free state. Since the minimum g value is quite distinct (Table VIII) from the other values for all three species, we looked initially for a correlation of its direction with vectors within the undamaged $HM(CO)_5^-$ moieties. A good correlation (Table IX) was found between the direction of g_{min} and either the perpendicular to the equatorial carbon plane of the anion or the bond from the metal atom to the axial carbon atom. Moreover, in the case of $W(CO)_5^-$, the direction of the intermediate $\mathbf{g}$ component lies within 2.4° of the equatorial W–C1 bond (Figure 2).

Table IX. Correlation between Tensor Principal Directions and Directions within the Undamaged Metal Carbonyl Anions

radical	tensor component	angle to M–C_5, deg[a]	angle from least-squares plane, deg[b]
$Cr(CO)_5^-$	g_{min}	8.8	6.0
$Mo(CO)_5^-$	g_{min}	4.7	4.8
	a_{max}	2.3	4.6
$W(CO)_5^-$	g_{min}	5.0	5.3

[a] Bond direction between metal atom and axial carbon atom. [b] Direction perpendicular to the least-squares plane for the four equatorial carbon atoms.

Hyperfine interaction with the metal nucleus was only detectable in the case of $PPN^+HMo(CO)_5^-$, where the direction of the maximum Mo hyperfine tensor component was very nearly parallel to that of g_{min} (Table IX). This conforms with the observations made for the $Cr(CO)_5^-$ and $W(CO)_5^-$ radicals in frozen glasses[22] and for the radical pair $[Cr(CO)_5^-]_2$ in $PPN^+HCr(CO)_5^-$[18] (see below). Powder spectra, of course, cannot provide the absolute directional information obtained from single-crystal studies. The present observation that g_{min} and a_{max} (at least for Mo) both lie, within experimental error, along the bond between the metal atom and the axial carbon atom (z direction) supports the earlier[18,22] contention that in this group of metal carbonyl radicals the unpaired electron is largely confined to a d_{z^2} metal orbital. Similar observations have been made[3,5,23] for the metal hyperfine interaction tensors in the square-pyramidal metal carbonyl radicals $Fe(CO)_5^+$, $Os(CO)_5^+$, and $Mn(CO)_5$. Furthermore, the results of extended Hückel calculations[1,24,25] support the experimentally observed geometry (C_{4v}) for these species and the assignment of a $^2A_1$ ground state.

In Figure 7 we reproduce the d-orbital scheme predicted for a d^7 square-pyramidal metal carbonyl.[1] In C_{4v} symmetry, first-order spin–orbit interactions between the ground a_1 (d_{z^2}) level and excited levels are restricted to the interaction with the filled degenerate e pair, which is permitted when the dc magnetic field lies in the equatorial

(22) Krusic, P. J. *J. Am. Chem. Soc.*, in press.

(23) Lionel, T.; Morton, J. R.; Preston, K. F. *J. Magn. Reson.* **1982**, *49*, 225.

(24) Elian, M.; Hoffmann, R. *Inorg. Chem.* **1975**, *14*, 1058.

(25) Burdett, J. K. *Adv. Inorg. Chem. Radiochem.* **1978**, *21*, 113.

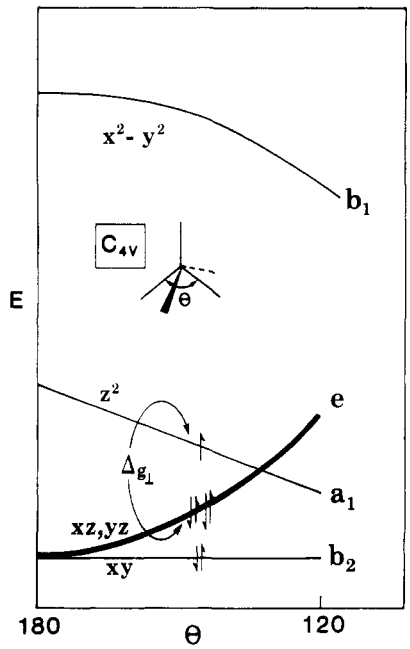

Figure 7. d-orbital scheme for square-pyramidal metal carbonyls, showing the symmetry-allowed g shift for a d^7 free radical (adapted from ref 1).

plane (xy). The proximity of the semioccupied level and the filled e level (Figure 7) then accounts for the large *positive* shift of the perpendicular components of **g** from the free-spin value (2.0023); the absence from the d-orbital scheme of a level of the requisite A_2 representation for spin–orbit interaction when B_0 is parallel to z results in a $g_\parallel$ value very close to the free-spin value, g_e. The observed increase in g shifts (Table VIII) with increasing atomic number is consistent with the first-order expressions[26] for the **g**-tensor components of a square-pyramidal d^7 species:

$$g_\parallel = g_e$$

$$g_\perp = g_e + 6\rho_a\rho_e\lambda/\Delta E$$

where ρ_a and ρ_e are the metal unpaired spin populations in d_{z^2} of the ground a_1 orbital and in $d_{xz,yz}$ of the excited e orbital, respectively. A small negative second-order contribution to all components of **g** from the a_1–e interaction[26] depends on λ^2 and presumably accounts for the steadily increasing negative $g_\parallel$ shift along the series Cr, Mo, W. Because the g shifts depend on unpaired spin densities in both ground and excited states and on the excitation energy, it is not too surprising that the observed shifts do not show a simple linear ($g_\perp$) or quadratic ($g_\parallel$) dependence on λ. There is some indication from the metal hyperfine tensors (see below) that the spin density in d_{z^2} increases with atomic number. This must be offset by a decrease in the metal spin density in the excited state and an increase in the excitation energy, since the dependences of the g shifts on λ are weaker than anticipated. The a_1–e excitation energy is closely related to the crystal field splitting, of course, and is therefore expected to increase considerably with atomic number. For $\rho_a = \rho_e = 0.5$, we estimate ΔE = 18000, 36000, and 44000 cm^{-1} for $Cr(CO)_5^-$, $Mo(CO)_5^-$, and $W(CO)_5^-$, respectively, from the above expressions and estimates of the spin–orbit coupling constants.[27]

Table X. Estimates of Hyperfine Parameters κ and P and Metal d_{z^2} Spin Densities for the $M(CO)_5^-$ Radicals

radical	κ^a	P^a	% d_{z^2}
$Cr(CO)_5^{-b}$	1.1	−63.6	62
$Mo(CO)_5^{-b}$	−42.3	−107.0	71
$W(CO)_5^-$	56.9	271.0	148

[a] Units of MHz. [b] Negative magnetic moments assumed.

In the present study, we have been able to observe hyperfine interaction of the unpaired electron with the central metal nucleus of $M(CO)_5^-$ for M = Mo only. However, the powder measurements of Krusic[22] and our measurements[28] made for the radical pairs in $PPh_4^+HM(CO)_5^-$ provide the metal hyperfine interaction tensors for Cr and W. For $Cr(CO)_5^-$, we estimate a nearly traceless axial ^{53}Cr tensor of (35.7, −17.4, −17.4 MHz), in fair accord with Krusic's isotropic measure of 1.4 G. For $W(CO)_5^-$, we estimate a ^{183}W tensor of (209, 0, 0 MHz), which agrees very well with the powder spectral measure of Krusic (69.5, ≅1, ≅1 G). Our present determination of the $^{95,97}Mo$ hyperfine interaction tensor (Table VI) also agrees well with his. The first-order expressions for the metal hyperfine tensor of a d^7 square-pyramidal species are[23,26,29]

$$a_\parallel = \kappa + P\rho_a\{4/7 - \Delta g_\perp/7\}$$

$$a_\perp = \kappa + P\rho_a\{-2/7 + 15\Delta g_\perp/14\}$$

where κ represents the sum of the s-orbital contributions, P is the one-electron dipolar parameter,[30] and ρ_a is the d_{z^2} spin density. The terms in $\Delta g_\perp$ represent the orbital magnetic moment contributions to the hyperfine interaction. Estimates of κ, P, and the d_{z^2} spin densities derived from theoretical one-electron parameters[30] are given in Table X. Dealing first with the κ values, we note that these correspond to 2% spin population in the metal valence s orbital at the most.[30] Metal s, p_z, and d_{z^2} contributions to the a_1 SOMO are symmetry-allowed, although calculations[24] for $Mn(CO)_5$ suggest that direct s character is limited to a few percent. Negative contributions to inner s orbitals from core polarization by the predominant d_{z^2} component will oppose the direct positive contributions, leading to the observed miniscule isotropic hyperfine interactions.[31] The spin populations estimated from the experimental $P\rho_a$ values clearly show the dominance of the d_{z^2} contribution to the SOMO in these radicals; however, there clearly is a problem associated with the estimate for tungsten. A similar problem arose in the case[23] of the $Os(CO)_5^+$ radical, where the estimated unpaired spin density in $Os(5d_{z^2})$ was considerably in excess of unity. Our[30] theoretical P values are evidently too small for the third-row transition elements, possibly through neglect of relativistic effects in the estimation of $\langle r^{-3}\rangle$. The observed trend toward higher spin density at the metal atom with increasing atomic number is expected as the d orbital becomes more energetic and makes a greater contribution to the antibonding SOMO.

The detection of a radical pair in $PPN^+HCr(CO)_5^-$ is not surprising in view of our previous observation that such radical pairs are formed in unusually high concentration relative to the monoradicals in certain radiation-damaged hydrido carbonyls.[18,28,32] In the present series of crystals,

(26) Reuveni, A.; Malatesta, V.; McGarvey, B. R. *Can. J. Chem.* **1977**, *55*, 70.
(27) Goodman, B. A.; Raynor, J. B. *Adv. Inorg. Chem. Radiochem.* **1970**, *13*, 135.
(28) Hynes, R.; Morton, J. R.; Preston, K. F.; Springs, J. J.; Williams, A. J. Unpublished data.
(29) Abragam, A.; Bleaney, B. *Electron Paramagnetic Resonance of Transition Ions*; Oxford University Press (Clarendon): Oxford, U.K., 1970; p 456.
(30) Morton, J. R.; Preston, K. F. *J. Magn. Reson.* **1978**, *30*, 577.
(31) Symons, M. C. R. *Chemical and Biochemical Aspects of Electron-Spin Resonance Spectroscopy*; Wiley: New York, 1978; p 124.

Table XI. Nearest-Neighbor[a] Cr–Cr Vectors in $PPN^+HCr(CO)_5^-$ and Corresponding Point Dipolar Interactions

Cr–Cr vector					
*a**	*b*	*c*	length, nm	symmetry operation[b]	$-D$, MHz
0.9769	0.0000	−0.2136	1.324	t	33.8
0.6893	0.6865	−0.2316	0.713	t + i	216.6
−0.8470	0.5169	0.1242	0.947	t + i	92.5
0.3819	0.7827	0.4914	1.287	t + C_2	36.8
0.0000	−0.5446	0.8387	0.951	t + σ	91.3

[a] For neighboring anion sites closer than 1.5 nm. [b] Symmetry operations connecting the two sites along the Cr–Cr vector: t, translation; σ, reflection; i, inversion; C_2, 2-fold rotation.

pair formation was evidently restricted to one rather weak species found in the chromium compound. It would appear that in these crystals the hydrogen atoms generated in the initial radiolytic or photolytic step can escape the immediate cage of nearest-neighbor anions in the $PPN^+HM(CO)_5^-$ lattice and abstract hydrogen atoms at remote anion sites. Alternatively, molecular hydrogen elimination and radical pair formation may still occur predominantly between nearest-neighboring anions, but electron exchange may not take place between the constituent radicals (i.e. $J = 0$). While this may seem a rather unlikely explanation, it cannot be entirely eliminated at present since the details of electron exchange in this type of crystal have yet to be ascertained. Our earlier[18,32] studies of radical pairs in organometallic crystals showed that such pairs are formed by antiferromagnetic coupling ($J > 0$) between a *very limited* number of possible combinations of nearest neighbors, to the near exclusion of monoradicals. Again, we note in this study that the $[Cr(CO)_5^-]_2$ pair detected in $PPN^+HCr(CO)_5^-$ is only one of many possible nearest-neighbor pairs (Table XI). Its nearly cylindrical spin–spin tensor (Table V) has a maximum principal value which lies only 5.7° from one of the intersite vectors (M_1–M_4 or M_2–M_3 in Figure 3) and which corresponds to a D value ($=3D_{zz}/2$) close to that expected (Table XI) for the appropriate point-dipolar interaction. Delocalization of the unpaired spin and spin–orbit contributions to the fine-structure tensor undoubtedly accounts for the small deviations of the tensor from axiality and from the crystallographic Cr–Cr direction. Interestingly, the triplet species observed does not correspond to the nearest possible pair of anions. Unfortunately, the weakness of the spectrum prevented a determination of the exchange parameter J from the temperature dependence of the line intensity. Since antiferromagnetic coupling is the established norm for such pairs,[18,28,32] we can safely assume that J is positive for this pair also.

The evidence that we have adduced here shows that the pentacarbonyl anions of the group 6 metals have square-pyramidal geometry and unpaired spin density principally located in the metal d_{z^2} atomic orbital. This geometry and electronic structure conform with those established[3-14] for the isoelectronic equivalents of groups 7 and 8. ^{13}C measurements[22] for $Cr(CO)_5^-$ and $Mo(CO)_5^-$ made in solution indicate that all five carbons are equivalent on the EPR time scale and demonstrate the participation of rapid fluxional motion in those species. Such rapid internal motion is a common feature of transition-metal carbonyls.

Acknowledgment. We wish to thank Dr. P. J. Krusic of the Du Pont Co., Wilmington, DE, for the provision of a preprint of his work on the group 6 pentacarbonyl anions and for many stimulating discussions. We are also indebted to Mr. R. Dutrisac of these laboratories for technical assistance.

Supplementary Material Available: Full tables of atomic coordinates and bond distances and angles for $PPN^+HW(CO)_5^-$ and tables of anisotropic thermal parameters for both rigid-body and full refinement (9 pages); tables of structure factors for both rigid-body and full refinement (41 pages). Ordering information is given on any current masthead page.

(32) Krusic, P. J.; Morton, J. R.; Preston, K. F.; Le Page, Y. *J. Mol. Struct.* **1988**, *189*, 1.